Interference in Finite-Sized Highly Dense Millimeter Wave Networks

Kiran Venugopal*, Matthew C. Valenti†, and Robert W. Heath, Jr.*
*The University of Texas, Austin, TX, USA.
† West Virginia University, Morgantown, WV, USA.
*{kiranv, rheath}@utexas.edu, †valenti@ieee.org

***Abstract*—The potential of millimeter wave (mmWave) frequencies for device-to-device communication among wearable electronics is enormous for applications requiring Gbps throughput. In a dense usage scenario such as inside a train car or airplane cabin, many devices may be present within close proximity where interference is significant. Previous work that models interference in wireless networks has leveraged stochastic geometry and often assumes an infinite number of interferers. In the indoor wearables setting, a finite network may be a more realistic assumption. This paper analyzes mmWave networks with a finite number of interferers that are located in fixed positions. The paper considers the effect of blockages, which are primarily caused by the human bodies present in the operating environment. Expressions for coverage and rate are developed, which capture the effects of key antenna characteristics such as directivity and gain.**

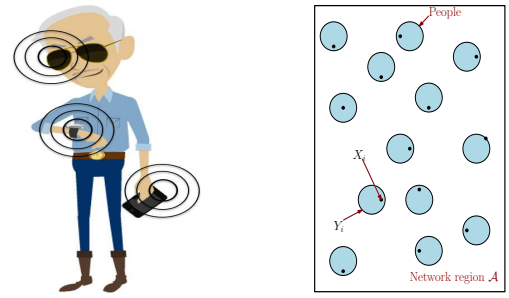

(a) Wearable communication network

(b) A train car

Fig. 1. Many users with wearable communication networks in (a) will be located in close proximity in a train car (b), creating mutual interference.

I. Introduction

Wearable communication networks are the next frontier for wireless communications [1]. Wearable networks connect different devices in and around the human body including low-rate devices like pedometers and high-rate devices like augmented-reality glasses. A main challenge for wearable networks is supporting high data rates in dense environments. The urban train car will be a particularly bad environment with many high-density wearable networks located in close proximity [2]. Understanding the interference environment is critical to understanding the rate, quality, and density that can be supported by wearable communication networks.

In this paper, we characterize the performance of millimeter wave (mmWave) wearable communication networks. Such networks might use wireless standards like IEEE 802.11ad [3], Wireless HD [4], or even device-to-device operating modes proposed for mmWave-based next-generation (5G) cellular systems [5], [6]. We focus on the performance of networks operating at the mmWave carrier frequency that are confined to a limited region and contain a finite number of interferers at fixed locations. We develop an approach for calculating coverage and rate in such a network. In crowded environments such as train cars or airline cabins, human bodies are a main and significant source of blockage of mmWave frequencies [7], [8]. As mmWave systems are likely to use compact antenna arrays, we assess the impact of antenna parameters, in particular the beamwidth and antenna gain, on the coverage and spectral efficiency of the system.

Prior work on mmWave-based networks has used results from stochastic geometry to analyze coverage and rate [9]–[11]. For analytical tractability, most work assumes an infinite number of mobile devices spread over an infinite area. These assumptions allow simplification through application of Campbell's theorem [12]. Analysis of the outage probability conditioned on the network geometry in ad hoc networks with a finite spatial extent and number of nodes was performed in [13], which was extended to the analysis of frequency-hopping networks in [14]. Compared with [9]–[14], we use the same computational approach as in [13], [14], with some similar assumptions on mmWave configuration and blockage from [9], [11], though we model people–not buildings– as blockages. An illustration of the finite network region and the wearable network is given in Fig. 1.

II. Network Topology and Signal Model

We consider a finite sized $2D$ network region $\mathcal{A}$ with a reference transmitter-receiver pair and K potentially interfering transmitters. The area of the network is denoted by $|\mathcal{A}|$, so that the interferer density $\lambda = K/|\mathcal{A}|$. The transmitters and their locations are denoted by X_i, $i = 0, 1, ..., K$, where X_0 is the reference transmitter location. We assume the reference receiver to be located at the origin and represent X_i as a complex number $X_i = R_i e^{j\phi_i}$, where $R_i = |X_i|$ is the distance to the ith transmitter and $\phi_i = \angle X_i$ is the angle to X_i from the reference receiver.

To model human body blockages, we treat each user as a circle of diameter W as illustrated in Fig. 1(b). These circles as well as the location of their centers are denoted by Y_i. In this blockage model, a transmitter X_i is blocked if the path

from X_i to the reference receiver intersects any Y_j or if X_i falls within a diameter-W circle of some blockage Y_j. In this paper, we ignore self-body blockage [8], so that a given user is not blocked by itself. If there are no blockages in the path from X_i to the reference receiver, then we say that the path is *line of sight* (LOS); otherwise, we say that it is *non-LOS* (NLOS). Blockages can be determined using the following algorithm:

1) Determine $\mathcal{L}$, the set of all transmitters X_i that have no blockages Y_j within a distance of $W/2$.
2) Sort the blockages from closest to most distant, so that $|Y_1| \leq |Y_2| \leq ... \leq |Y_K|$. Let the corresponding angles relative to the receiver be $\angle Y_1,\ \angle Y_2,\ ...,\ \angle Y_K$.
3) For each $i \in \{1,\ 2,\ ...,\ K\}$, compute the *blocking cones (wedge in 2D)*[1] B_{C_i} as

$$B_{C_i} = \angle Y_i \pm \tan^{-1}\left(\frac{W}{2|Y_i|}\right). \tag{1}$$

4) For each $\ell \in \mathcal{L}$, determine if X_ℓ is blocked by checking to see if it lies within any blocking cone; i.e., if

$$\phi_\ell \in \bigcup_{\{i:|Y_i|<R_\ell\}} B_{C_i}. \tag{2}$$

To facilitate analysis, we use a sectorized antenna model [9, Fig. 1(b)]. The beamwidth of the antenna main-lobe at the transmitter is θ_t and at the receiver is θ_r. The main-lobe gain of the transmitter is G_t and the receiver is G_r. Similarly, the back-lobe gains are denoted as g_t and g_r. To parameterize our pattern, we assume that a uniform planar square array (UPA) with half-wavelength antenna element spacing is used at the transmitters and the receiver. The number of antenna elements at the transmitter and receiver are denoted as N_t and N_r, respectively. The values for the beamwidth, main-lobe and back-lobe gains for an N element (i.e. $\sqrt{N} \times \sqrt{N}$) UPA is given in Table I. Because our system model is built in a $2D$ world, the beamwidth is determine by $\sqrt{N}$ but the main-lobe gain is proportional N (assuming it is aligned in both azimuth and elevation) while the side-lobe gain depends on the reciprocal of N (assuming both azimuth and elevation are not aligned). A model that incorporates 3D would also include orientation of the antennas at the expense of a more elaborate and less tractable model. When the number of antenna elements is one, we say that the UPA is omni-directional for which the main-lobe and side-lobe gains are unity. As in [9], [10], we assume that each interferer is transmitting with its main-lobe pointed in a random direction.

The fade gain h_i from X_i to the reference receiver is assumed to be Gamma distributed (Nakagami fading). We use m_i to denote the Nakagami factor for X_i which takes value m_L for LOS and m_N for NLOS. The path-loss exponent for X_i is denoted as α_i where $\alpha_i = \alpha_\mathsf{L}$ if X_i is LOS and $= \alpha_\mathsf{N}$ if it is NLOS. We use σ^2 to denote the noise power divided by the reference transmitter power as measured at unit reference distance (with no antenna gains). The transmit power of X_i is denoted as P_i. We assume an Aloha-like medium-access protocol and that each interferer transmits with probability p_t, which is assumed to be the same for all interferers.

[1]Strictly speaking, a blocking cone is an instance of a truncated cone because it does not extend to the origin.

TABLE I
ANTENNA PARAMETERS OF A UNIFORM PLANAR SQUARE ANTENNA

Number of antenna elements	N
Beamwidth θ	$\frac{2\pi}{\sqrt{N}}$
Main-lobe gain G	N
Side-lobe gain g	$\frac{1}{\sin^2\left(\frac{3\pi}{2\sqrt{N}}\right)}$

The fade gain h_0 of the reference communication link is also Nakagami with parameter m_0. We assume that the reference link is always communicating using LOS. Of course, it is possible that the body itself will create blockages on the reference link in a wearable network. Modeling this self-blockage and incorporating the results into the analysis is an interesting topic for future work.

It is important to note that the boundaries of the finite area are assumed to be impenetrable, so there is no leakage of external interference into the finite area. Further, reflections due to the boundary and people are not explicitly incorporated in the model. They are accounted for only in a coarse way in the different LOS and NLOS model parameters, which ideally would be determined based on ray tracing or measurement results.

III. INTERFERENCE MODEL

Conditioned on the network (meaning the locations of the transmitters and blockages), we can find the complementary cumulative distribution function (CCDF) of the signal to interference plus noise ratio (SINR) (also called SINR coverage probability in [9]) by adapting the analysis in [13]- [14]. We define a discrete random variable I_i for $i = \{1, ..., K\}$ that represents the relative power radiated by X_i in the direction of the reference receiver. With probability $(1 - p_\mathsf{t})$, X_i does not transmit at all, and hence $I_i = 0$. Otherwise, the relative power will depend on whether or not the random orientation of X_i's antenna is such that the reference receiver is within the main-lobe. We assume a uniform orientation of X_i's antenna, and thus the probability that the reference receiver is within its main-lobe is $\frac{\theta_\mathsf{t}}{2\pi}$. It follows that

$$I_i \quad = \quad \begin{cases} 0 & \text{with probability } (1-p_\mathsf{t}) \\ G_\mathsf{t} & \text{with probability } p_\mathsf{t}\left(\frac{\theta_\mathsf{t}}{2\pi}\right) \\ g_\mathsf{t} & \text{with probability } p_\mathsf{t}\left(1-\frac{\theta_\mathsf{t}}{2\pi}\right) \end{cases}. \tag{3}$$

We can justify randomizing the orientation angles of the interferers because: (1) the user itself may be randomly moving the orientation of her devices while using them, and (2) the user may have a wearable network with several devices with different orientations and random activity (though we assume the medium access protocol of the wearable network allows only one of the user's devices to transmit at a time). Note that

a similar approach was used in [14] for modeling adjacent-channel interference in frequency hopping: when the interferer transmitted, one of two power compensations was applied depending on whether the interferer hopped into the same or an adjacent channel.

Now, let us define the normalized power gain from X_i to be

$$\Omega_i = \begin{cases} \frac{P_i}{P_0} G_{\mathsf{r}} R_i^{-\alpha_i} & \text{if } -\frac{\theta_{\mathsf{r}}}{2} \leq \phi_i - \phi_0 \leq \frac{\theta_{\mathsf{r}}}{2} \\ \frac{P_i}{P_0} g_{\mathsf{r}} R_i^{-\alpha_i} & \text{otherwise} \end{cases}, \quad (4)$$

where $\alpha_i = \alpha_{\mathsf{N}}$ if X_i is NLOS and $\alpha_i = \alpha_{\mathsf{L}}$ if X_i is LOS. The SINR is

$$\gamma = \frac{h_0 \Omega_0}{\sigma^2 + \sum_{i=1}^{K} I_i h_i \Omega_i}, \quad (5)$$

where $\Omega_0 = G_{\mathsf{r}} R_0^{-\alpha_0}$ is the normalized power gain from the reference transmitter, as we assume the reference transmitter is always within the main beam of the reference receiver.

IV. Coverage Probability

Denoting $\mathbf{\Omega} = [\Omega_0, ..., \Omega_K]$, the coverage probability $P_{\mathsf{c}}(\beta)$ for a given $\mathbf{\Omega}$ is defined as the CCDF of the SINR evaluated at a threshold β and is given by

$$P_{\mathsf{c}}(\beta) = \mathbb{P}\left[\gamma > \beta | \mathbf{\Omega}\right]. \quad (6)$$

Substituting (5) into (6) and rearranging leads to

$$P_{\mathsf{c}}(\beta) = \mathbb{P}\left[\mathsf{S} > \sigma^2 + \sum_{i=1}^{K} \mathsf{Y}_i \,\middle|\, \mathbf{\Omega}\right], \quad (7)$$

where

$$\mathsf{S} = \beta^{-1} h_0 \Omega_0, \quad \mathsf{Y}_i = I_i h_i \Omega_i. \quad (8)$$

Conditioned on $\mathbf{\Omega}$, let $f_{\mathbf{Y}}(\mathbf{y})$ denote the joint probability density function (pdf) of $(\mathsf{Y}_1, ..., \mathsf{Y}_K)$ and $f_{\mathsf{S}}(s)$ denote the pdf of S. Then, (7) can be written as

$$P_{\mathsf{c}}(\beta) = \int_{\mathbb{R}^K} ... \int \left(\int_{\sigma^2 + \sum_{i=1}^{K} y_i}^{\infty} f_{\mathsf{S}}(s) \mathrm{d}s \right) f_{\mathbf{Y}}(\mathbf{y}) \mathrm{d}\mathbf{y}. \quad (9)$$

Defining, $\beta_0 = \beta m_0 / \Omega_0$, the random variable S is gamma distributed with pdf given by

$$f_{\mathsf{S}}(s) = \frac{(\beta_0)^{m_0}}{(m_0 - 1)!} s^{m_0 - 1} e^{-\beta_0 s}, \; s \geq 0. \quad (10)$$

Using (10) and assuming that m_0 is a positive integer, the inner integral in (9) is

$$\int_{\sigma^2 + \sum_i^K y_i}^{\infty} f_{\mathsf{S}}(s) \mathrm{d}s = e^{-\beta_0 (\sigma^2 + \sum_i^K y_i)} \times \sum_{\ell=0}^{m_0 - 1} \frac{(\beta_0 \sigma^2)^{\ell}}{\ell!} \left(1 + \frac{1}{\sigma^2} \sum_{i}^{K} y_i\right)^{\ell}. \quad (11)$$

Substituting (11) into (9) leads to

$$P_{\mathsf{c}}(\beta) = e^{-\beta_0 \sigma^2} \sum_{\ell=0}^{m_0 - 1} \frac{(\beta_0 \sigma^2)^{\ell}}{\ell!} \times \int_{\mathbb{R}^K} ... \int e^{-\beta_0 \sum_{i=1}^{K} y_i} \left(1 + \frac{1}{\sigma^2} \sum_{i=1}^{K} y_i\right)^{\ell} f_{\mathbf{Y}}(\mathbf{y}) \mathrm{d}\mathbf{y}. \quad (12)$$

Using the binomial theorem followed by multinomial expansion,

$$\begin{aligned} \left(1 + \frac{1}{\sigma^2} \sum_{i=1}^{K} y_i\right)^{\ell} &= \sum_{t=0}^{\ell} \binom{\ell}{t} \left(\frac{1}{\sigma^2} \sum_{i=1}^{K} y_i\right)^{t} \\ &= \sum_{t=0}^{\ell} \binom{\ell}{t} \frac{t!}{\sigma^{2t}} \sum_{\substack{t_i \geq 0 \\ \sum_{i=1}^{K} t_i = t}} \left(\prod_{i=1}^{K} \frac{y_i^{t_i}}{t_i!}\right), \end{aligned} \quad (13)$$

where the last summation is over the set of $\{t_i\}$ that sum to t. Substituting (13) into (12) gives

$$P_{\mathsf{c}}(\beta) = e^{-\beta_0 \sigma^2} \sum_{\ell=0}^{m_0 - 1} \frac{(\beta_0 \sigma^2)^{\ell}}{\ell!} \sum_{t=0}^{\ell} \binom{\ell}{t} \frac{t!}{\sigma^{2t}} \sum_{\substack{t_i \geq 0 \\ \sum_{i=1}^{K} t_i = t}} \int_{\mathbb{R}^K} ... \int \prod_{i=1}^{K} \frac{y_i^{t_i}}{t_i!} e^{-\beta_0 y_i} f_{\mathbf{Y}}(\mathbf{y}) \mathrm{d}\mathbf{y}. \quad (14)$$

Given $\mathbf{\Omega}$, $\{\mathsf{Y}_i\}_{i=1}^{K}$ are independent. So, $f_{\mathbf{Y}}(\mathbf{y})$ can be written as $\prod_{i=1}^{K} f_{\mathsf{Y}_i}(y_i)$, where

$$\begin{aligned} f_{\mathsf{Y}_i}(y_i) = \; & p_{\mathsf{t}} \left(\frac{m_i}{\Omega_i}\right)^{m_i} \frac{y_i^{m_i - 1}}{\Gamma(m_i)} \left[\frac{\theta_{\mathsf{t}}}{2\pi} \frac{e^{-\frac{m_i y_i}{G_{\mathsf{t}} \Omega_i}}}{G_{\mathsf{t}}^{m_i}} + \right. \\ & \left. \left(1 - \frac{\theta_{\mathsf{t}}}{2\pi}\right) \frac{e^{-\frac{m_i y_i}{g_{\mathsf{t}} \Omega_i}}}{g_{\mathsf{t}}^{m_i}} \right] u(y_i) + (1 - p_{\mathsf{t}}) \, \delta(y_i), \end{aligned} \quad (15)$$

$\delta(y_i)$ is the Dirac delta function, and $u(y_i)$ is the unit step function. Further, based on $\mathbf{\Omega}$, the Nakagami parameter m_i in (15) is either m_{L} if LOS or m_{N} if NLOS. Using (15), the joint pdf in (14) can be simplified and written as follows

$$P_{\mathsf{c}}(\beta) = e^{-\beta_0 \sigma^2} \sum_{\ell=0}^{m_0 - 1} \frac{(\beta_0 \sigma^2)^{\ell}}{\ell!} \sum_{t=0}^{\ell} \binom{\ell}{t} \frac{t!}{\sigma^{2t}} \sum_{\substack{t_i \geq 0 \\ \sum_{i=1}^{K} t_i = t}} \left(\prod_{i=1}^{K} \mathcal{G}_{t_i}(\Omega_i)\right), \quad (16)$$

where (using (15))

$$\begin{aligned} \mathcal{G}_{t_i}(\Omega_i) = & \int \frac{y_i^{t_i}}{t_i!} e^{-\beta_0 y_i} f_{\mathsf{Y}_i}(y_i) dy_i \\ = & \, p_{\mathsf{t}} \left(\frac{\Omega_i}{m_i}\right)^{t_i} \frac{\Gamma(m_i + t_i)}{t_i! \Gamma(m_i)} \left[\frac{\theta_{\mathsf{t}}}{2\pi} \psi_{t_i}(G_{\mathsf{t}}) \right. \\ & \left. + \left(1 - \frac{\theta_{\mathsf{t}}}{2\pi}\right) \psi_{t_i}(g_{\mathsf{t}}) \right] + (1 - p_{\mathsf{t}}) \, \delta[t_i]. \end{aligned} \quad (17)$$

TABLE II
ANTENNA PARAMETERS

Number of antenna elements	1	4	16
Beam width in degrees	360	49.6	24.8
Main-lobe gain in dB	0	6	12
Back-lobe gain in dB	0	3	0.7

In (17), $\delta[t_i]$ is the Kronecker delta function defined as

$$\delta[t_i] = \begin{cases} 1 & \text{if } t_i = 0 \\ 0 & \text{if } t_i \neq 0 \end{cases} \tag{18}$$

and

$$\psi_{t_i}(x) = x^{t_i}\left(1 + \frac{\beta_0 x \Omega_i}{m_i}\right)^{-(m_i+t_i)}. \tag{19}$$

V. ERGODIC SPECTRAL EFFICIENCY

When the SINR is β, the spectral efficiency is

$$\eta = \log_2(1+\beta). \tag{20}$$

The CCDF of the spectral efficiency is found by defining the equivalent events

$$\{\gamma > \beta\} \Leftrightarrow \underbrace{\{\log_2(1+\gamma) > \eta\}}_{\{\gamma > 2^\eta - 1\}}. \tag{21}$$

The event on the left corresponds to the coverage probability $P_{\mathsf{c}}(\beta)$, while the event on the right corresponds to the CCDF of the spectral efficiency, $P_\eta(r)$, also called the *rate coverage probability*. Since equivalent, the two events have the same probability, and it follows that

$$P_\eta(r) = P_{\mathsf{c}}\left(2^r - 1\right). \tag{22}$$

See also Lemma 5 of [9].

Using the fact that for a non-negative X, $\mathbb{E}[X] = \int_0^\infty (1 - F(x))\mathsf{d}x$ (see (5-33) in [15]), the *ergodic spectral efficiency* can be found from

$$\mathbb{E}[\eta] = \int_0^\infty P_{\mathsf{c}}\left(2^r - 1\right)\mathsf{d}r \tag{23}$$

$$= \frac{1}{\log(2)}\int_0^\infty \frac{P_{\mathsf{c}}(\beta)}{1+\beta}\mathsf{d}\beta, \tag{24}$$

where the last line uses the change of variables $\beta = 2^r - 1 \rightarrow \mathsf{d}r = \frac{1}{\log(2)}\mathsf{d}\beta/(1+\beta)$.

VI. NUMERICAL RESULTS

In this section, we summarize the numerical results for coverage probability and ergodic spectral efficiency when the nodes are located in a regular 5 × 9 rectangular grid - a typical scenario would be where the lattice points (users) are separated by 2 ft, in which case, $|\mathcal{A}|$ =10 ft × 18 ft. Since the locations of the K transmitters are fixed, we let X_i = Y_i. The reference transmitter is located at a distance d_0 from the reference receiver and the minimum distance of two nodes in the grid is $2d_0$. It is assumed that the P_i are all the same; i.e., all transmitters transmit at the same power.

TABLE III
PARAMETERS USED TO OBTAIN NUMERICAL RESULTS FOR FIXED GEOMETRY

Parameters	Values
d_0	1
m_{L}	4
m_{N}	2
α_{L}	2
α_{N}	4
W	1
σ^2	-20 dB
K	44

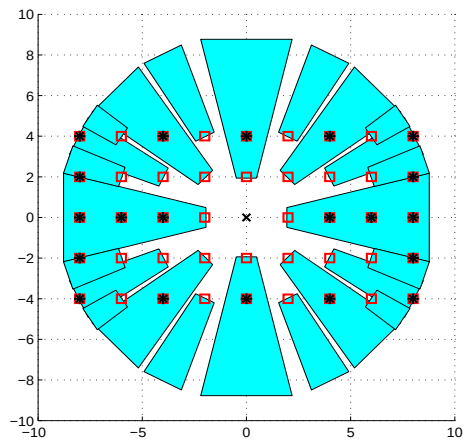

Fig. 2. The locations of the nodes in a uniform grid of size 5 × 9 and the blocking cones when the reference receiver is at the center. The blocked nodes are indicated as filled.

The values of the antenna beamwidth, main-lobe and back-lobe gains are summarized in Table II. The parameters used to obtain the results in this section are summarized in Table III. Note that since the reference receiver is assumed to be located at one of the grid locations, the total number of interfering nodes K is 44. With $d_0 = 1$, as given in Table III, this would mean that the interferer density $\lambda = 0.244$, so that the network is very dense and approximates the peak-hour passenger load [2]. We consider two locations for the reference receiver: (1) the center of the grid - because the grid is 5 × 9, we have an exact center which is a valid lattice point; and (2) a corner point of the grid.

The case when the reference receiver is located at the center of the grid is shown in Fig. 2. The nodes are indicated using squares and the blocking wedges resulting from the node locations are also shown. The blocked nodes are indicated by filled squares. A similar plot when the reference receiver is located at one of the corner points is shown in Fig. 3.

The dependence of coverage probability on the transmission probability p_{t} of the interferers for a fixed transmitter and receiver antenna array configuration is shown in Fig. 4 for the case when the reference receiver is located at the center and both the transmitters and the receiver use omni-directional antenna. It is seen that, as expected, higher the value of p_{t} smaller the coverage probability for a given SINR threshold. We observe similar results for the case when the receiver is located at a corner and for other antenna configurations.

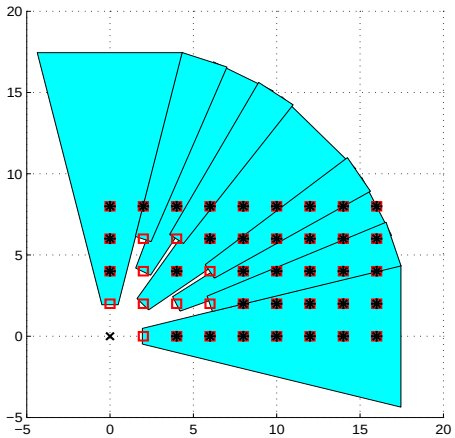

Fig. 3. The locations of the nodes in a uniform grid of size 5×9 and the blocking cones when the reference receiver is at a corner. The blocked nodes are indicated as filled.

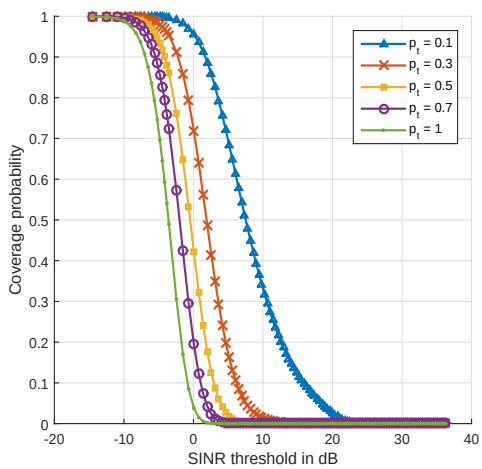

Fig. 4. Coverage probability vs SINR threshold for different transmission probability p_t for the interferers when the receiver is located at the center and both the transmitters and receiver use omni-directional antennas.

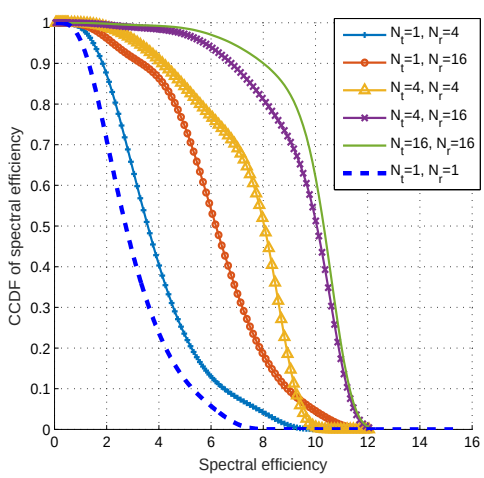

Fig. 5. CCDF of spectral efficiency for different antenna configurations. Receiver located at center, receiver antenna orientation $\phi_0 = 0^o$ and $p_t = 0.1$.

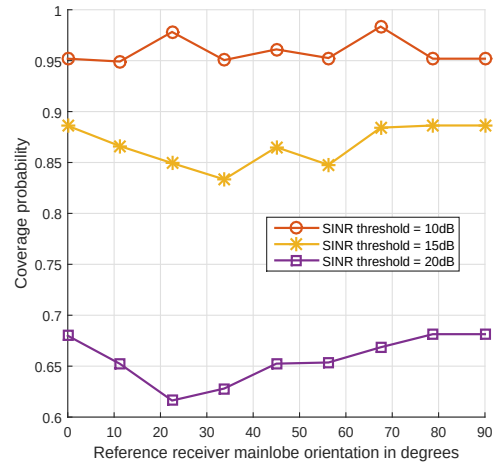

(a) Receiver at the center

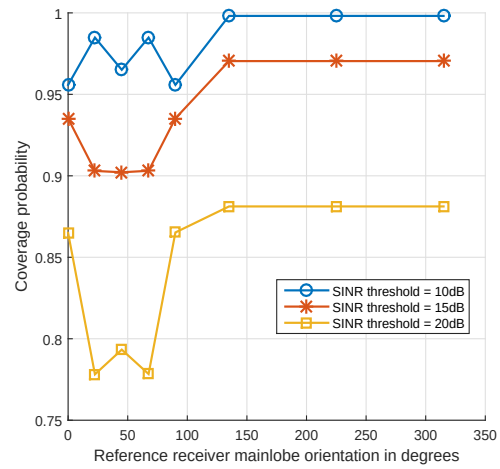

(b) Receiver at the corner $(0, 0)$

Fig. 6. Plot of coverage probability against reference receiver antenna orientation for various SINR thresholds when $p_t = 0.7$ and a 16-element antenna array is used at the transmitters and the receiver.

The CCDF of spectral efficiency for different antenna configurations is shown in Fig. 5 for a given transmission probability. Here we let $p_t = 0.1$ and fix the orientation of the receiver antenna main-lobe $\phi_0 = 0^o$ for comparison. The effect of orientation angle of the reference receiver antenna main-lobe is shown in Fig. 6 for three separate SINR thresholds. We fix the antenna sizes at the transmitters and the receiver and let $p_t = 0.7$. It is observed that the influence of orientation angle of the receiver is more pronounced when the reference receiver is located at a corner rather than at the center. When the antennas are oriented away from the interfering users (orientation angles more than 90° in Fig. 6(b)) the coverage probability is higher as expected, for the case when the receiver is located at the corner $(0, 0)$.

The ergodic spectral efficiency for various antenna configurations when the reference receiver orientation is $\phi_0 = 0^o$ and $p_t = 1$ are summarized in Table IV. It can be seen that the performance is better when the reference receiver

TABLE IV
ERGODIC SPECTRAL EFFICIENCY FOR VARIOUS ANTENNA CONFIGURATIONS

N_t	N_r	Ergodic spectral efficiency	
		Receiver at center	Receiver at a corner
1	1	0.499	1.063
1	4	0.797	1.405
1	16	1.757	2.087
4	1	2.449	4.046
4	4	3.210	5.072
4	16	5.437	7.078
16	1	3.618	5.027
16	4	4.635	6.396
16	16	6.952	8.434

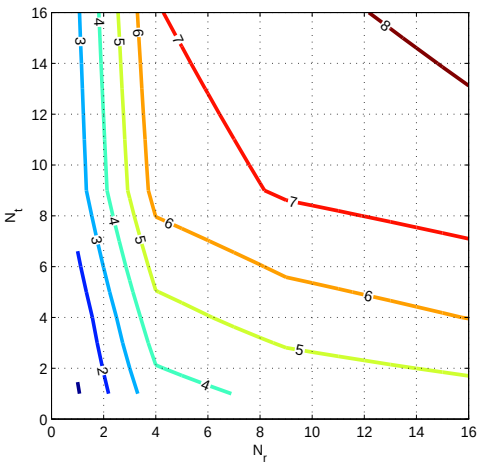

Fig. 7. Contour plot of ergodic spectral efficiency as a function of N_t and N_r. Receiver located at center, receiver antenna orientation $\phi_0 = 0^o$ and $p_t = 0.5$.

is located at a corner rather than at the center. Also, having larger N_t is more advantageous than having a larger N_r. This can also be seen from Fig. 7 which is a contour plot of the ergodic spectral efficiency as a function of N_t and N_r for a fixed receiver antenna orientation $\phi_0 = 0^o$ and transmission probability $p_t = 0.5$.

VII. CONCLUSION

In this paper, we analyzed the performance of a mmWave wearable communication network operating in a finite region like that inside a train car. We assumed fixed positions for the interfering nodes and assessed the impact of antenna parameters such as array gain and beamwidth on coverage and ergodic spectral efficiency of the system. We observed a significant improvement in coverage probability with larger antenna arrays, and having more transmit antennas is more advantageous than having more receive antennas. We also observed that the effect of orientation of the receive antenna array is more profound for users located at a corner region rather than at the center. In future work, it would be interesting to consider the interferers at random locations and derive closed form expressions for the spatially averaged coverage and ergodic spectral efficiency. Further refinements to the model would also be useful including accounting body-blockage of the reference communication link and more explicit incorporation of 3D antenna orientations.

VIII. ACKNOWLEDGEMENT

This work was supported in part by the Intel 5G program. M.C. Valenti was supported by the Big-XII Faculty Fellowship program. The authors would like to thank Salvatore Talarico for his programming assistance.

REFERENCES

[1] "Smart wearable devices: Fitness, healthcare, entertainment & enterprise 2013-2018," *Juniper Research*, Oct. 2013.
[2] "Railway Passenger Vehicle Capacity, An overview of the way railway vehicle capacity has evolved." http://www.railway-technical.com/Infopaper%202%20Railway%20Passenger%20Vehicle%20Capacity%20v1.pdf.
[3] E. Perahia, C. Cordeiro, M. Park, and L. Yang, "IEEE 802.11ad: Defining the next generation multi-gbps wi-fi," *Consumer Communications and Networking Conference (CCNC), 2010 7th IEEE.*, pp. 1–5, Jan. 2010.
[4] "WirelessHD specification overview." http://www.wirelesshd.org/wp-content/uploads/2009/12/WirelessHD-Specification-Overview-v1-0-4-Aug09.pdf, Aug. 2009.
[5] F. Boccardi, R. W. Heath Jr., A. Lozano, T. Marzetta, and P. Popovski, "Five disruptive technology directions for 5G," *IEEE Commun. Magazine*, vol. 52, pp. 74–80, Feb. 2014.
[6] T. Rappaport *et al*, "Millimeter wave mobile communications for 5G cellular: It will work!," *IEEE Access*, vol. 18, pp. 335–349, 2013.
[7] J. S. Lu, D. Steinbach, P. Cabrol, and P. Pietraski, "Modeling human blockers in millimeter wave radio links," *ZTE Communications*, vol. 10, pp. 23–28, Dec. 2012.
[8] T. Bai and R. W. Heath Jr., "Analysis of self-body blocking effects in millimeter wave cellular networks," in *Proc. Asilomar Conf. Signals, Systems, Computers*, Nov. 2014.
[9] T. Bai and R. W. Heath Jr., "Coverage and rate analysis for millimeter wave cellular networks," *IEEE Trans. Wireless Comm.*, 2014. in press, preprint available at http://dx.doi.org/10.1109/TWC.2014.2364267.
[10] S. Singh, M. N. Kulkarni, A. Ghosh, and J. G. Andrews, "Tractable model for rate in self-backhauled millimeter wave cellular networks," *ArXiv e-prints*, July 2014. ArXiv document number: 1407.5537.
[11] T. Bai, A. Alkhateeb, and R. W. Heath Jr., "Coverage and capacity of millimeter-wave cellular networks," *IEEE Commun. Magazine*, vol. 52, pp. 70–77, Sep. 2014.
[12] M. Haenggi and R. K. Ganti, *Interference in large wireless networks*. Now Publishers, 2009.
[13] D. Torrieri and M. C. Valenti, "The outage probability of a finite ad hoc network in Nakagami fading," *IEEE Trans. Commun.*, vol. 60, pp. 3509–3518, Nov. 2012.
[14] M. C. Valenti, D. Torrieri, and S. Talarico, "Adjacent-channel interference in frequency-hopping ad hoc networks," in *Proc. IEEE Int. Conf. on Commun. (ICC)*, pp. 5583–5588, June 2013.
[15] A. Papoulis and S. U. Pillai, *Probability, Random Variables and Stochastic Processes, Fourth Edition*. McGraw Hill, 2002.